Electronic Supplmentary Information for: Large polarons in two-dimensional fullerene networks: The crucial role of anisotropy in charge transport†

T. S. A. Cassiano[a], M. L. Pereira Junior[*,b], G. M. e Silva[aa], P. H. de Oliveira Neto[a] and L. A. Ribeiro Junior[*a,c]

[a] *University of Brasília, Institute of Physics, 70.910-900, Brasília, Brazil*
[b] *University of Brasília, Faculty of Technology, Department of Electrical Engineering, 70910-900, Brasília, Brazil.*
[c] *Computational Materials Laboratory, LCCMat, Institute of Physics, University of Brasília, 70910-900, Brasília, Brazil ribeirojr@unb.br**

1 Selecting the best parameters

To determine the parameters of H, we initially focus on the intermolecular coupling constant. Through a preliminary scan using the stationary algorithm, we observed that stable polarons are obtained when α_{inter} is approximately 20-30% of α_{intra}. This range of values ensures that a wide range of $J_0^{x/y}$ values leads to stable polarons with similar properties. Configurations with α_{inter} below this range exhibit weak intermolecular interactions, which are insufficient to sustain a localized structure. Conversely, higher values result in excessively high polaron formation energies, rendering them unrealistic. Therefore, we have chosen the value of 0.765 eV/Å to represent the non-local electron-phonon coupling constant for $qHPC_{60}$.

Figure S1 illustrates the IPR (a) and E_p (b) heatmaps, which depict the variations of these quantities with respect to J_0^x and the hopping integral ratio J_0^y/J_0^x. The degree of isotropy in the lattice increases with a higher ratio value. In Figure S1(a), the yellow region represents low IPR values, while the blue-toned areas indicate high IPR measurements. It is evident that the effect of promoting isotropy depends on the magnitude of the x-direction hopping integral, J_0^x. When J_0^x falls within the range of 150-200 meV, a slight increase in J_0^y leads to a corresponding increase in IPR. However, for J_0^x values exceeding this threshold, IPR exhibits a slight initial increase but ultimately decreases as J_0^y is further increased.

For instance, when $J_0^X = 150$ meV, the IPR increases from 0.48 to 0.62 as J_0^y is increased. On the other hand, in the case of $J_0^X = 300$ meV, the IPR initially rises with J_0^y but suddenly drops to zero in a highly isotropic regime. The specific ratio between the two hopping integrals at which this transition occurs depends on the magnitude of J_0^x. When $J_0^x = 225$ meV, the IPR is close to zero only at the isotropic limit ($J_0^y = J_0^x$). However, for $J_0^x = 300$ meV, an anisotropy level of just 50% ($J_0^y = 0.5J_0^x$) is sufficient to yield the same outcome. This trend is a direct consequence of the energy balance of the electronic and lattice components.

As J_0^y increases, the electronic energy also increases, disrupting the balance with the lattice energy required to form a stable polaron. This preference for large polarons ultimately leads to the emergence of band-like delocalized solutions when the hopping integrals reach significant magnitudes.

A detailed examination of the E_p heatmap (Figure S1(b)) confirms this observation. In this heatmap, warm colors represent configurations with higher polaron formation energies, while cool colors indicate lower values of E_p. As anticipated, the energies are influenced by variations in J_0^x. Specifically, larger values of this parameter result in higher values of E_p. This response can be attributed to the functional form of Eq. 14, where E_p exhibits a linear dependence on the hopping integrals.

Increasing either J_0^x or J_0^y leads to an increase in energy [1]. At high levels of isotropy, where the contributions from the x and y directions are combined, the energy is higher. This interplay results in three distinct regions in the parameter space, characterized by nearly constant values of E_p: a blue, a green, and a red region. The first two regions correspond to physically realistic carriers, while the last region exhibits extremely high E_p values that render stable polaron formation unfeasible. Consequently, one can conclude that the formation of stationary and stable polarons is achievable in monolayer fullerene networks.

Further increases in J_0^x will only lead to the formation of nonphysical carriers with even higher values of E_p at lower levels of isotropy. Based on this observation, we can conclude that pushing this parameter beyond 300 meV does not enhance the description of the charge carriers in $qHPC_{60}$. Instead, it restricts the

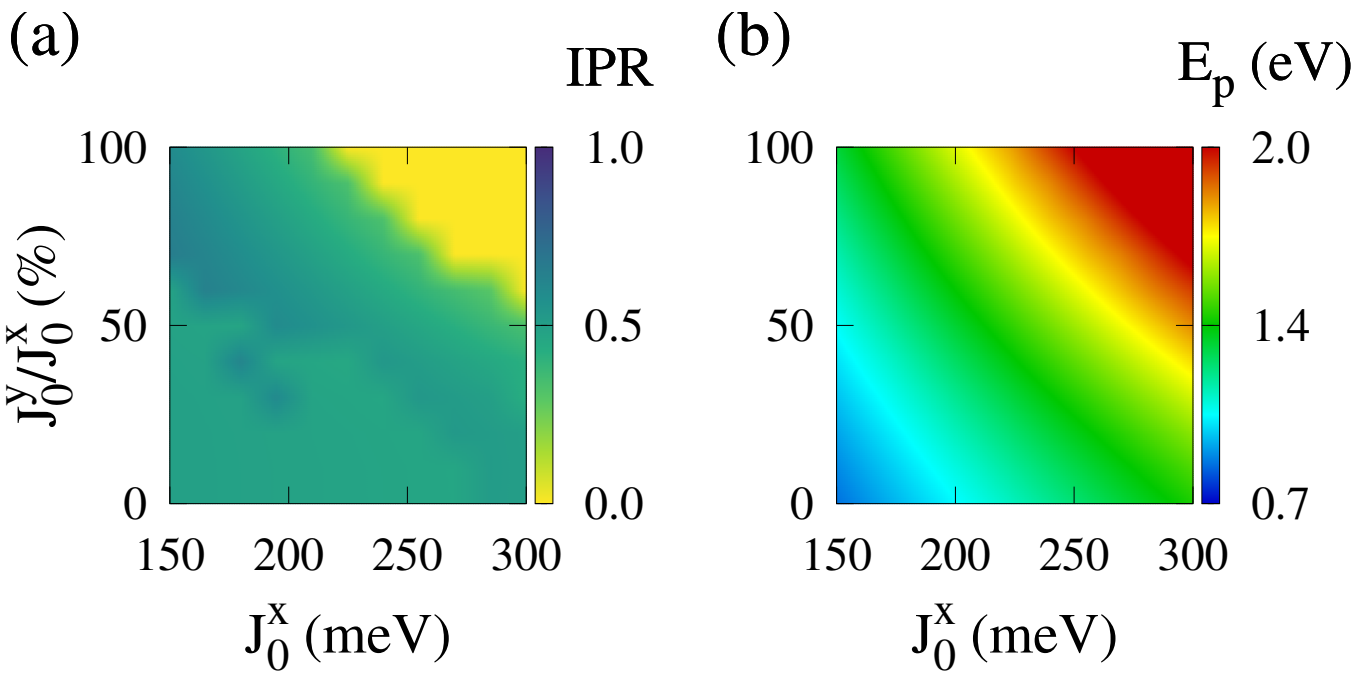

Figure S1: Stationary properties of polarons in model qHPC$_{60}$ are examined as a function of J_0^x and J_0^y/J_0^x. Panel (a) presents the IPR heatmap, where yellow regions correspond to configurations with low IPR and blue regions indicate high IPR measurements. In panel (b), the polaron formation energy is depicted. Hot colors represent high E_p, while cold tones indicate low E_p values.

available range of isotropy levels. As a reasonable compromise to accurately represent the material, we will constrain the parameter to an upper limit of 250 meV in the subsequent analysis.

Interestingly, a strong correlation between E_p and IPR becomes evident when comparing the two heatmaps. Areas with high polaron energy correspond to low IPR values, indicating a clear relationship between the two properties. Furthermore, configurations with moderate to low E_p values (ranging from 0.6 eV to 1.5 eV) exhibit IPR values between 0.45 and 0.60. This trend suggests that, within the model, large polarons are more appropriate for describing the charge carriers in fullerene networks, as highly delocalized solutions result in unrealistically high values of E_p.

As mentioned earlier, we will restrict J_0^x to 200-250 meV going forward. The lower limit is estimated based on the calculated hopping integrals of a typical OMC held together by weak van der Waals interactions, where $J_0^{x/y}$ values are typically around 50-100 meV [2, 3, 4, 5]. Strong covalent bridge bonds connect the sites in the network. Therefore, the corresponding J_0^x value should reflect the distinction between the two types of molecular arrangements.

2 Effect of anisotropy on polaron morphology

To gain insight into the effect of anisotropy on carrier properties, we examine the electronic and lattice structures of polarons in three distinct regimes. Figures S2(a) and S2(d) illustrate the lattice arrangement and charge density profile of the network in the isotropic case. Similarly, Figures S2(b) and S2(e) depict the same interplay for the scenario where $J_0^y = 0.5J_0^x$, while Figures S2(c) and S2(f) represent the case with $J_0^y = 0.2J_0^x$. In Figures S2(a), S2(b), and S2(c), the lattice distribution is depicted by black disks organized in a square grid.

Each site in the lattice represents a molecular unit, identified by its row (i) and column (j) coordinates, as shown in Figure 1. The size of the disks in the lattice diagram indicates the magnitude of the associated $u_{i,j}$. Thus, larger disks represent C$_{60}$ molecules that have expanded from their undisturbed internal lattice configuration, while smaller disks indicate contraction. Additionally, each molecule is connected to its four

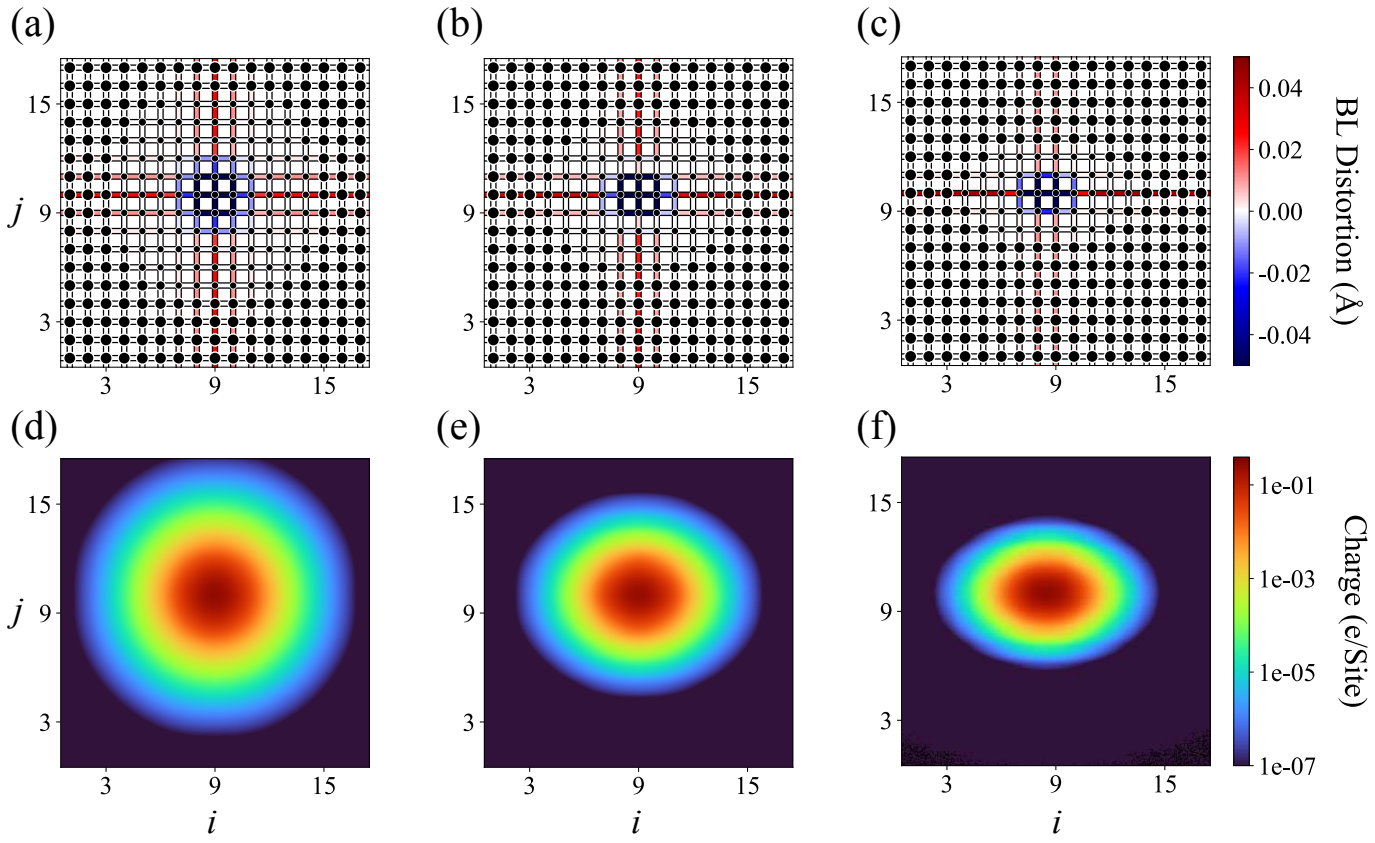

Figure S2: The morphological properties of the polaron in three anisotropy regimes are depicted. Figures (a)-(c) illustrate the lattice arrangement of the model qHPC$_{60}$ for $J_0^y/J_0^x = 1$, $J_0^y/J_0^x = 0.5$, and $J_0^y/J_0^x = 0.2$, respectively. The size of the disks indicates the magnitude of $u_{i,j}$, while the colors of the links connecting the sites indicate the extent of bond length distortion around a_0: red and blue represent expansion and contraction, respectively. Figures (d)-(f) show the corresponding charge density profiles of the configurations. In these figures, cold and red colors stand low and high local charge densities, respectively.

neighboring molecules via bond links. The colors of these links indicate the distortions in bond length ($\Delta x_{i,j}$ and $\Delta y_{i,j}$) relative to the lattice parameter a_0. Bonds depicted in red have expanded, blue represents contraction, and white links experienced no change in length.

In the isotropic configuration shown in Figure S2(a), a distinct radial region can be observed, centered around the site ($i = 9$,$j = 10$), where all the sites have undergone contraction to a similar extent. Additionally, the bonds surrounding the central sites are uniformly depicted in blue. The intensity of their distortions increases as they approach the molecule at ($i = 9$,$j = 10$). Moving away from this central area, three red signals emerge in each cardinal direction, extending to the network's edges. These red signals represent the combined effects of inter- and intramolecular lattice deformations, forming the phonon cloud associated with the polaron.

The observed symmetry between the x and y directions is a natural consequence of the isotropic hopping integral, making the model Hamiltonian invariant under exchanges between the two directions. Corresponding to the circular shape of the polaron's internal lattice deformation, the charge density exhibits a similar profile, characterized by a radial distribution originating from the center of the model qHPC$_{60}$. The size of this distribution is approximately equivalent to the region delimited by the contracted sites in Figure S2(a), highlighting the coupled nature of the carrier.

In isotropic configurations, the hosted polarons exhibit significant transport inertia. This can be attributed to several factors. Firstly, the imposed symmetry results in equivalent directions for the polaron delocalization, eliminating any preferential path for transport. Moreover, the polaron is a composite entity consisting of phonon clouds and localized charge accumulation, necessitating their collective movement. As the lattice deformations extend throughout the entire lattice in the isotropic case, the energy required to mobilize the polaron becomes substantial. In other words, the carrier possesses a high effective mass. Similar findings were observed in previous studies investigating polaron stability in other materials, such as OMCs [6, 7].

This physical picture undergoes a notable transformation with the introduction of anisotropy, as depicted in Figure S2(b) with $J_0^y = 0.5J_0^x$. In this scenario, the degree of intramolecular lattice deformations diminishes (as the number of compressed discs decreases), rendering an ellipsoid-like shape. This trend aligns with the intermolecular deformation pattern along the x-direction, which becomes more localized in the molecular line where most of the polaron charge is concentrated. A similar lattice deformation profile is observed in Figure S2(c), but with an even more concentrated ellipsoid-like pattern. Consequently, it can be inferred that by imposing anisotropy, the lattice deformations concentrate the polaron in a preferred direction (a specific molecular line), reducing transport inertia.

This feature becomes apparent when looking at the configuration with 20% of anisotropy, as shown in Figure S2(c). Only 17 bonds near the center display some degree of contraction, in contrast to the 40 ones observed in Figure S2(a). Moreover, the vertically aligned expansions are less distorted, displaying lighter red tones. This relaxation in the y-direction is compensated by the emergence of strongly stretched bonds along the horizontal line of the central site (i.e., the molecule that concentrates most of the polaron charge).

The degree of anisotropy in the polaron directly influences the strength of deformations along the direction with a lower transfer integral, which in this case is the y-direction. As the anisotropy increases, these deformations become weaker. Consequently, the energy barrier for charge transport decreases, promoting a more favorable charge transport mechanism. Similar conclusions have been drawn from recent studies on OMCs [6]. This anisotropic behavior holds for any value of J_0^x within the range of 200-250 meV, indicating that anisotropy is essential for an accurate physical description of the model qHPC$_{60}$. Without anisotropy, the charge carriers would exhibit nonphysical high effective masses.

We emphasize that the model lattice presents a high degree of anisotropy, and hopping integrals can vary from 50-250 meV depending on the carrier transport direction within the basal plane. It also corroborates the choice of our model for the square lattice.

References

[1] Marcelo Lopes Pereira Junior, Rafael Timóteo de Sousa Júnior, Geraldo Magela e Silva, and Luiz Antônio Ribeiro Júnior. Stationary polaron properties in organic crystalline semiconductors. Physical Chemistry Chemical Physics, 21(5):2727–2733, 2019.

[2] Eung-Gun Kim, Veaceslav Coropceanu, Nadine E Gruhn, Roel S Sánchez-Carrera, Robert Snoeberger, Adam J Matzger, and Jean-Luc Brédas. Charge transport parameters of the pentathienoacene crystal. Journal of the American Chemical Society, 129(43):13072–13081, 2007.

[3] Motonori Watanabe, Yuan Jay Chang, Shun-Wei Liu, Ting-Han Chao, Kenta Goto, Md Minarul Islam, Chih-Hsien Yuan, Yu-Tai Tao, Teruo Shinmyozu, and Tahsin J Chow. The synthesis, crystal structure and charge-transport properties of hexacene. Nature chemistry, 4(7):574–578, 2012.

[4] Marcelo Lopes Pereira Jr, Wiliam Ferreira da Cunha, Rafael Timóteo de Sousa Jr, Geraldo Magela e Silva, and Luiz Antonio Ribeiro Jr. Stationary and dynamical properties of polarons in anisotropic c60-crystals. The Journal of Physical Chemistry C, 123(22):13410–13418, 2019.

[5] Elham Mozafari and Sven Stafström. Polaron dynamics in a two-dimensional holstein-peierls system. The Journal of chemical physics, 138(18):184104, 2013.

[6] Luiz Antonio Ribeiro Junior and Sven Stafström. Polaron dynamics in anisotropic holstein–peierls systems. Physical Chemistry Chemical Physics, 19(5):4078–4084, 2017.

[7] Luiz Antonio Ribeiro Junior and Sven Stafström. Polaron stability in molecular semiconductors: Theoretical insight into the impact of the temperature, electric field and the system dimensionality. Physical Chemistry Chemical Physics, 17(14):8973–8982, 2015.